

Limits to compression with cascaded quadratic soliton compressors

M. Bache,^{1,*} O. Bang,¹ W. Krolikowski,^{1,2} J. Moses,³ and F. W. Wise⁴

¹*DTU Photonics, Technical University of Denmark, Bld. 345v, DK-2800 Lyngby, Denmark*

²*Research School of Physical Sciences and Engineering, Australian National University, Canberra ACT 0200, Australia*

³*Optics and Quantum Electronics Group, Massachusetts Institute of Technology, Cambridge, MA 02139*

⁴*Department of Applied and Engineering Physics, Cornell University, Ithaca, New York 14853*

bache@com.dtu.dk

November 1, 2018

Abstract: We study cascaded quadratic soliton compressors and address the physical mechanisms that limit the compression. A nonlocal model is derived, and the nonlocal response is shown to have an additional oscillatory component in the nonstationary regime when the group-velocity mismatch (GVM) is strong. This inhibits efficient compression. Raman-like perturbations from the cascaded nonlinearity, competing cubic nonlinearities, higher-order dispersion, and soliton energy may also limit compression, and through realistic numerical simulations we point out when each factor becomes important. We find that it is theoretically possible to reach the single-cycle regime by compressing high-energy fs pulses for wavelengths $\lambda = 1.0 - 1.3 \mu\text{m}$ in a β -barium-borate crystal, and it requires that the system is in the stationary regime, where the phase mismatch is large enough to overcome the detrimental GVM effects. However, the simulations show that reaching single-cycle duration is ultimately inhibited by competing cubic nonlinearities as well as dispersive waves, that only show up when taking higher-order dispersion into account.

© 2018 Optical Society of America

OCIS codes: 320.5520, 320.7110, 190.5530, 190.2620, 320.2250

References and links

1. G. P. Agrawal, *Applications of nonlinear fiber optics* (Academic Press, London, 2001).
2. L. F. Mollenauer, R. H. Stolen, and J. P. Gordon, "Experimental Observation of Picosecond Pulse Narrowing and Solitons in Optical Fibers," *Phys. Rev. Lett.* **45**, 1095–1098 (1980).
3. S. Ashihara, J. Nishina, T. Shimura, and K. Kuroda, "Soliton compression of femtosecond pulses in quadratic media," *J. Opt. Soc. Am. B* **19**, 2505–2510 (2002).
4. S. Ashihara, T. Shimura, K. Kuroda, N. E. Yu, S. Kurimura, K. Kitamura, M. Cha, and T. Taira, "Optical pulse compression using cascaded quadratic nonlinearities in periodically poled lithium niobate," *Appl. Phys. Lett.* **84**, 1055–1057 (2004).
5. J. A. Moses, J. Nees, B. Hou, K.-H. Hong, G. Mourou, and F. W. Wise, "Chirped-Pulse Cascaded Quadratic Compression of 1-mJ, 35-fs Pulses with Low Wavefront Distortions," In *Conference on Lasers and Electro-Optics*, p. CTuS5 (Optical Society of America, 2005).
6. J. Moses and F. W. Wise, "Soliton compression in quadratic media: high-energy few-cycle pulses with a frequency-doubling crystal," *Opt. Lett.* **31**, 1881–1883 (2006).
7. J. Moses, E. Alhammali, J. M. Eichenholz, and F. W. Wise, "Efficient High-Energy Femtosecond Pulse Compression in Quadratic Media with Flattop Beams," *Opt. Lett.* **32**, 2469–2471 (2007).
8. X. Zeng, S. Ashihara, N. Fujioka, T. Shimura, and K. Kuroda, "Adiabatic compression of quadratic temporal solitons in aperiodic quasi-phase-matching gratings," *Opt. Express* **14**, 9358–9370 (2006).

9. G. Xie, D. Zhang, L. Qian, H. Zhu, and D. Tang, "Multi-stage pulse compression by use of cascaded quadratic nonlinearity," *Opt. Commun.* **273**, 207–213 (2007).
10. M. Bache, O. Bang, J. Moses, and F. W. Wise, "Nonlocal explanation of stationary and nonstationary regimes in cascaded soliton pulse compression," *Opt. Lett.* **32**, 2490–2492 (2007), arXiv:0706.1933.
11. M. Bache, J. Moses, and F. W. Wise, "Scaling laws for soliton pulse compression by cascaded quadratic nonlinearities," *J. Opt. Soc. Am. B* **24**, 2752–2762 (2007), arXiv:0706.1507.
12. R. DeSalvo, D. Hagan, M. Sheik-Bahae, G. Stegeman, E. W. Van Stryland, and H. Vanherzeele, "Self-focusing and self-defocusing by cascaded second-order effects in KTP," *Opt. Lett.* **17**, 28–30 (1992).
13. C. B. Clausen, O. Bang, and Y. S. Kivshar, "Spatial Solitons and Induced Kerr Effects in Quasi-Phase-Matched Quadratic Media," *Phys. Rev. Lett.* **78**, 4749–4752 (1997).
14. X. Liu, L. Qian, and F. W. Wise, "High-energy pulse compression by use of negative phase shifts produced by the cascaded $\chi^{(2)} : \chi^{(2)}$ nonlinearity," *Opt. Lett.* **24**, 1777–1779 (1999).
15. P. Di Trapani, A. Bramati, S. Minardi, W. Chinaglia, C. Conti, S. Trillo, J. Kilius, and G. Valiulis, "Focusing versus Defocusing Nonlinearities due to Parametric Wave Mixing," *Phys. Rev. Lett.* **87**, 183902 (2001).
16. L. Bergé, O. Bang, J. J. Rasmussen, and V. K. Mezentsev, "Self-focusing and solitonlike structures in materials with competing quadratic and cubic nonlinearities," *Phys. Rev. E* **55**, 3555–3570 (1997).
17. W. Krolikowski, O. Bang, N. Nikolov, D. Neshev, J. Wyller, J. Rasmussen, and D. Edmundson, "Modulational instability, solitons and beam propagation in spatially nonlocal nonlinear media," *J. Opt. B: Quantum Semiclass. Opt.* **6**, s288 (2004).
18. F. Ö. Ilday, K. Beckwitt, Y.-F. Chen, H. Lim, and F. W. Wise, "Controllable Raman-like nonlinearities from nonstationary, cascaded quadratic processes," *J. Opt. Soc. Am. B* **21**, 376–383 (2004).
19. N. I. Nikolov, D. Neshev, O. Bang, and W. Krolikowski, "Quadratic solitons as nonlocal solitons," *Phys. Rev. E* **68**, 036614 (2003).
20. J. Moses and F. W. Wise, "Controllable Self-Steepening of Ultrashort Pulses in Quadratic Nonlinear Media," *Phys. Rev. Lett.* **97**, 073903 (2006), see also arXiv:physics/0604170.
21. V. Dmitriev, G. Gurzadyan, and D. Nikogosyan, *Handbook of Nonlinear Optical Crystals*, Vol. 64 of *Springer Series in Optical Sciences* (Springer, Berlin, 1999).
22. W. Krolikowski and O. Bang, "Solitons in nonlocal nonlinear media: Exact solutions," *Phys. Rev. E* **63**, 016610 (2000).
23. M. Bache, O. Bang, and W. Krolikowski, (2008), in preparation.
24. A. W. Snyder and D. J. Mitchell, "Accessible Solitons," *Science* **276**, 1538–1541 (1997).
25. W. Krolikowski, O. Bang, J. J. Rasmussen, and J. Wyller, "Modulational instability in nonlocal nonlinear Kerr media," *Phys. Rev. E* **64**, 016612 (2001).
26. I. V. Shadrivov and A. A. Zharov, "Dynamics of optical spatial solitons near the interface between two quadratically nonlinear media," *J. Opt. Soc. Am. B* **19**, 596–602 (2002).
27. N. Akhmediev and M. Karlsson, "Cherenkov radiation emitted by solitons in optical fibers," *Phys. Rev. A* **51**, 2602–2607 (1995).
28. D. V. Skryabin, F. Luan, J. C. Knight, and P. S. J. Russell, "Soliton Self-Frequency Shift Cancellation in Photonic Crystal Fibers," *Science* **301**, 1705–1708 (2003).
29. I. Cristiani, R. Tediosi, L. Tartara, and V. Degiorgio, "Dispersive wave generation by solitons in microstructured optical fibers," *Opt. Express* **12**, 124–135 (2003).
30. K. C. Chan and M. S. F. Liu, "Short-pulse generation by higher-order soliton-effect compression: Effects of fiber characteristics," *IEEE J. Quant. Elect.* **31**, 2226–2235 (1995).
31. K.-T. Chan and W.-H. Cao, "Improved soliton-effect pulse compression by combined action of negative third-order dispersion and Raman self-scattering in optical fibers," *J. Opt. Soc. Am. B* **15**, 2371–2376.
32. M. Bache, H. Nielsen, J. Lægsgaard, and O. Bang, "Tuning quadratic nonlinear photonic crystal fibers for zero group-velocity mismatch," *Opt. Lett.* **31**, 1612–1614 (2006), arXiv:physics/0511244.

1. Introduction

Compression of optical pulses can be achieved by first inducing a nonlinear phase shift on the pulse by self-phase modulation (SPM) from the cubic nonlinear response of, e.g., an optical fiber [1]. The phase shift creates a chirp across the pulse, which means that compression can subsequently be achieved in a dispersive material (such as a grating pair). In cubic soliton compressors both the SPM induced chirp and the compression is achieved in the same material [2]. The self-focusing cubic nonlinearity requires anomalous dispersion to compress the pulse. Due to collapse problems this limits the energy of the compressed pulse, and the requirement of anomalous dispersion restricts the accessible wavelength regime for soliton compression.

Recent progress has shown that cascaded quadratic soliton compressors (CQSCs) may ef-

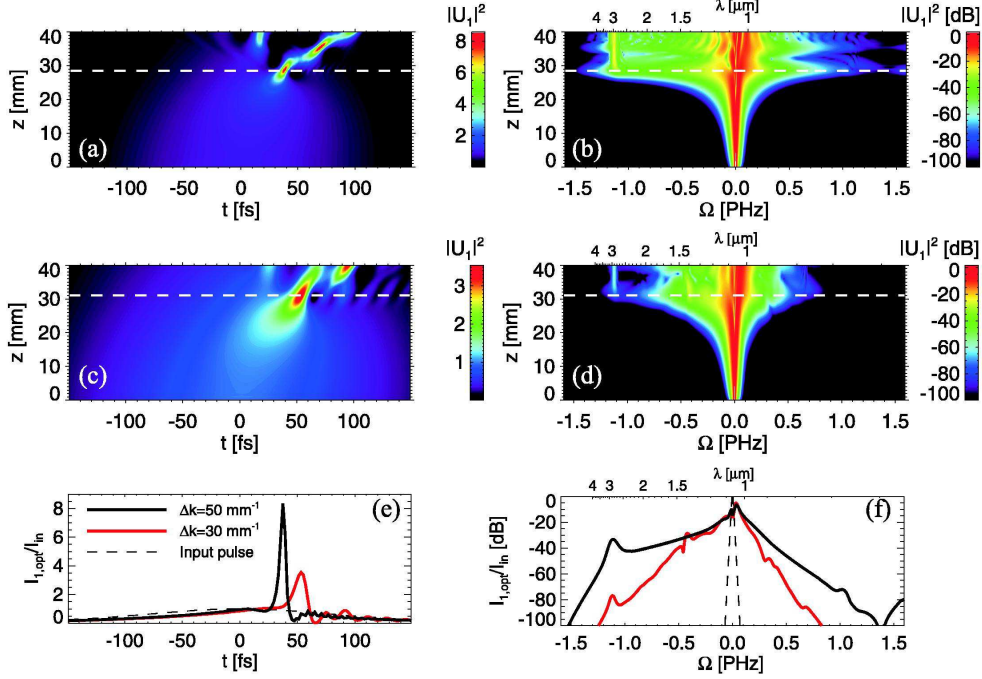


Fig. 1. Numerical simulations of soliton compression of a 200 fs FWHM pulse in a BBO crystal pumped at $\lambda_1 = 1064$ nm with a soliton number of $N_{\text{eff}} = 8$. (a) and (b) Temporal and spectral components of the FW $|U_1|^2 = I_1/I_{\text{in}}$ in the stationary regime ($\Delta k = 50 \text{ mm}^{-1}$, $I_{\text{in}} = 59 \text{ GW/cm}^2$). The pulse is compressed to 6 fs at the optimal compression point [$z = z_{\text{opt}}$, dashed line, cuts in (e) and (f)]. (c) and (d) In the nonstationary regime ($\Delta k = 30 \text{ mm}^{-1}$, $I_{\text{in}} = 29 \text{ GW/cm}^2$), a 17 fs pulse compressed pulse with trailing oscillations is observed.

fectively compress high-energy fs pulses down to ultra-short few-cycle pulses [3–11]. Here the nonlinear phase shift is induced due to phase-mismatched second-harmonic generation (SHG), which acts as a cascaded quadratic nonlinear process. The pump, or fundamental wave (FW), experiences an effective SPM from the cyclic energy transfer to the second harmonic (SH). The advantage is that the effective cubic nonlinearity induced by the cascading process can be made self-defocusing because it is controlled by the sign of the phase-mismatch parameter [12–15], and therefore normal dispersion can be used to compress the FW.

As this compressor scheme exploits an effective self-defocusing cubic term from cascaded quadratic effects, the compressor will naturally be affected by the self-focusing cubic nonlinearity inherent to any transparent material. This detrimental cubic nonlinearity must be counterbalanced and then exceeded to achieve compression [3, 6, 11, 14]. Furthermore, the propagation in a bulk medium having self-focusing cubic nonlinear response can avoid collapse problems if the self-defocusing cascaded nonlinearity is strong enough [16]. Thus, this compressor works in a bulk configuration even with multi-mJ input pulse energies [14].

Experimentally, compression of mJ pulses was observed at near-infrared wavelengths of 800 nm from 120 fs down to 30 fs when the compression was done externally (using either a prism pair or a near-lossless block of bulk calcite) [14] and when working as a soliton compressor from 120 fs to 45 fs [3] and from 35 fs to 20 fs [5]. In an important recent advance, spatially uniform compression using super-Gaussian flat-top beams was demonstrated also at 800

nm [7]. At 1260 nm compression to 12 fs (3 optical cycles) was achieved [6], while at telecom wavelengths compression down to 35 fs was observed [4, 8]. Numerical simulations have predicted sub-2-cycle pulses, but it was clear already in the first experiments that group-velocity mismatch (GVM) was a limiting factor for compression [6, 14]. It was observed that in the so-called *stationary regime* clean compression is possible, while in the so-called *nonstationary regime* GVM distorts the compressed pulse too much to be of any practical use, and severe reductions in compression capabilities is observed. As an example of this, the numerical simulations in Figs. 1(a)-(b) and Figs. 1(c)-(d) compare the pulse compression performance under equal conditions in the two regimes. In the stationary regime a 6 fs compressed pulse is observed while the nonstationary regime the GVM effects are much stronger, resulting in a 17 fs compressed pulse with trailing oscillations.

Significant progress in understanding this was recently made by using nonlocal theory (see Ref. [17] for a review on optically nonlocal media). The GVM-induced Raman-like term found previously [6, 18] was shown to originate from a temporally nonlocal response function [10]. The nonlocal behaviour appears when approximating the phase-mismatched dispersive SHG process in the cascading limit as a nonlinear convolution between the FW and a nonlocal response function [19]. An accurate prediction of when the system is stationary or nonstationary was presented, and the nonlocal theory predicted that an oscillatory chirp was created on the FW for short enough pulses in the nonstationary regime, which effectively limits the amount of compression achievable and qualitatively explained the trailing oscillations observed. It was also argued that the temporal time scales of the nonlocal response function had an influence on the final compressed pulse duration, but a systematic investigation was not made.

On the other hand, a recent study showed that the performance of the CQSC can conveniently be described by scaling laws involving an effective soliton number $N_{\text{eff}}^2 = N_{\text{SHG}}^2 - N_{\text{Kerr}}^2$, appearing as the difference between the quadratic and the cubic soliton numbers [11]. Since N_{eff} depends only on input parameters (such as parameters describing the input pulse intensity and duration and the material), the compressed pulse properties can be predicted using these scaling laws. Appropriate input parameters can then be found giving compression to single-cycle duration. However, neither the experiments nor the numerical simulations have ever observed single-cycle compression, so obviously there are higher order effects that prevent compression to reach such levels. In particular, both experiments and simulations found optimal phase mismatch values, where the best compression is observed. It is the purpose of the present theoretical and numerical analysis to discover what defines these optimal operation points.

2. Propagation equations

The SHG propagation equations in the slowly-evolving wave-approximation (SEWA) are used to study pulses in a bulk quadratic nonlinear crystal with single-cycle temporal resolution. Neglecting diffraction as well as the non-instantaneous cubic Raman response the dimensionless equations for the FW (ω_1) and SH ($\omega_2 = 2\omega_1$) fields $U_{1,2}(\xi, \tau)$ are [11, 20]

$$(i\partial_\xi + \hat{D}'_1)U_1 + |\Delta k'|^{1/2}N_{\text{SHG}}\hat{S}'_1U_1^*U_2e^{i\Delta k'\xi} + N_{\text{Kerr}}^2\hat{S}'_1U_1(|U_1|^2 + B\bar{n}|U_2|^2) = 0, \quad (1a)$$

$$(i\partial_\xi - id'_{12}\partial_\tau + \hat{D}'_{2,\text{eff}})U_2 + |\Delta k'|^{1/2}N_{\text{SHG}}\hat{S}'_2U_1^2e^{-i\Delta k'\xi} + 2\bar{n}^2N_{\text{Kerr}}^2\hat{S}'_2U_2(|U_2|^2 + B\bar{n}^{-1}|U_1|^2) = 0. \quad (1b)$$

Higher order dispersion (HOD) is included through the operator $\hat{D}'_j \equiv \sum_{m=2}^{m_d} i^m \delta_j^{(m)} \frac{\partial^m}{\partial \tau^m}$, with the dimensionless dispersion coefficients $\delta_j^{(m)} \equiv k_j^{(m)}(T_{\text{in}}^{m-2}|k_1^{(2)}|m!)^{-1}$ and $k_j^{(m)} \equiv \partial^m k_j / \partial \omega^m|_{\omega=\omega_j}$. Since $k_j = n_j \omega_j / c$ is known analytically through the Sellmeier equations of [21], the exact dispersion $\hat{D}_j = k_j(\omega) - (\omega - \omega_j)k_1^{(1)} - k_j(\omega_j)$ is used in the numerics [11],

corresponding to a dispersion order $m_d = \infty$. n_j is the refractive index, and the phase mismatch of the SHG process is $\Delta k = k_2 - 2k_1$. The Kerr cross-phase modulation (XPM) term $B = 2$ for type 0 SHG while for type I SHG $B = 2/3$ [11]. The time coordinate moves with the FW group velocity $v_{g,1} = 1/k_1^{(1)}$, giving the GVM term $d_{12} = v_{g,1}^{-1} - v_{g,2}^{-1}$. The equations are reported in dimensionless form, $\tau = t/T_{\text{in}}$, where T_{in} is the FW input pulse duration, $\xi = z/L_{D,1}$, where $L_{D,1} = T_{\text{in}}^2/|k_1^{(2)}|$ is the FW dispersion length, and finally $U_1 = E_1/\mathcal{E}_{\text{in}}$ and $U_2 = E_2/\sqrt{\bar{n}}\mathcal{E}_{\text{in}}$. Here \mathcal{E}_{in} is the amplitude of the peak electric input field, $\bar{n} = n_1/n_2$, $d'_{12} = d_{12}T_{\text{in}}/|k_1^{(2)}|$, and $\Delta k' = \Delta k L_{D,1}$. This scaling gives the quadratic (SHG) and cubic (Kerr) soliton numbers [6, 11]

$$N_{\text{SHG}}^2 = \frac{L_{D,1}\mathcal{E}_{\text{in}}^2\omega_1^2 d_{\text{eff}}^2}{c^2 n_1 n_2 |\Delta k|}, \quad N_{\text{Kerr}}^2 = \frac{L_{D,1} n_{\text{Kerr},1} \mathcal{E}_{\text{in}}^2 \omega_1}{c} \quad (2)$$

where d_{eff} is the effective quadratic nonlinearity, and $n_{\text{Kerr},j} = 3\text{Re}(\chi^{(3)})/8n_j$ is the cubic (Kerr) nonlinear refractive index. N_{SHG} might seem poorly defined in Eqs. (1) because of the factor $|\Delta k'|^{1/2}$ in front of it, but the choice will become clear later. Self-steepening is included through the operators $\hat{S}'_j \equiv 1 + i(\omega_j T_{\text{in}})^{-1} \frac{\partial}{\partial \tau}$. The combination of self-steepening and GVM implies that in the SEWA framework the SH dispersion effectively is given by $\hat{D}'_{2,\text{eff}} = \hat{D}'_2 + \hat{S}'_2^{-1} \frac{v}{2} \frac{\partial^2}{\partial \tau^2}$, where $v \equiv cd_{12}^2/\omega_2 n_2 |k_1^{(2)}|$ [11, 20]. We stress that all primed symbols in our notation are the dimensionless form of the corresponding unprimed symbol.

3. Nonlocal model: reduced equation in the cascading limit

The CQSC works in the cascading limit, *i.e.*, $|\Delta k'| \gg 1$, and we henceforth take $\Delta k' > 0$ as to have a self-defocusing cascaded nonlinearity. In order to support solitons we then need normal group-velocity dispersion (GVD), *i.e.*, $k_j^{(2)} > 0$. We now seek to reduce the full SEWA model (1), in order to get some physical insight into the compression process. In Ref. [10] it was shown that in the cascading limit Eqs. (1) can be reduced to a single equation for the FW

$$\left[i \frac{\partial}{\partial \xi} - \frac{1}{2} \frac{\partial^2}{\partial \tau^2} \right] U_1 + N_{\text{Kerr}}^2 U_1 |U_1|^2 - N_{\text{SHG}}^2 U_1^* \int_{-\infty}^{\infty} ds R_{\pm}(s) U_1^2(\xi, \tau - s) = 0. \quad (3)$$

In this derivation both self-steepening and HOD were neglected ($\hat{S}_j = 1$, $m_d = 2$), but as shown later this can straightforwardly be relaxed. Additionally the Kerr XPM terms were neglected. This dimensionless generalized nonlinear Schrödinger equation (NLSE) shows that the cascaded quadratic nonlinearity imposes a temporal nonlocal response on the FW, governed by the nonlocal response functions R_{\pm} [examples are shown in Fig. 2(a,c)]. This model quantified the previous qualitative definitions [14, 18] of the stationary and nonstationary regimes. When $d_{12}^2 > 2\Delta k k_2^{(2)}$ the system is in the nonstationary regime and the oscillatory response function R_- must be used. The criterion can be interpreted using characteristic length scales, giving $L_{\text{GVM}}^2 < L_{\text{coh}} L_{D,2}/2\pi$; when GVM dominates its length scale $L_{\text{GVM}} = T_{\text{in}}/|d_{12}|$ becomes shorter than one controlled by the product of the coherence length $L_{\text{coh}} = \pi/|\Delta k|$ and the SH GVD length scale $L_{D,2} = T_{\text{in}}^2/|k_2^{(2)}|$. When $d_{12}^2 < 2\Delta k k_2^{(2)}$ the system is in the stationary regime and one has to use the localized response function R_+ . We will now derive this result in details.

In the cascading limit $\Delta k' \gg 1$ the nonlocal approach takes the ansatz

$$U_2(\xi, \tau) = \phi_2(\tau) \exp(-i\Delta k' \xi) \quad (4)$$

This ansatz is assuming that all the dynamics in the propagation direction of the SH is dominated by the phase mismatch, and the condition for making this ansatz is that the coherence

length $L_{\text{coh}} = \pi/\Delta k$ is much shorter than any other characteristic length scale. This is true in the cascading limit except when the FW is extremely short, in which case the GVM length $L_{\text{GVM}} = T_{\text{in}}/|d_{12}|$ can become on the order of L_{coh} . Assuming $N_{\text{Kerr}}^2 U_2 \ll \Delta k^{1/2} N_{\text{SHG}}$ we may discard the Kerr terms in Eq. (1b), and get an ordinary differential equation (ODE)

$$\delta_2^{(2)} \frac{d^2 \phi_2}{d\tau^2} + id'_{12} \frac{d\phi_2}{d\tau} - \Delta k' \phi_2 = \Delta k'^{1/2} N_{\text{SHG}} U_1^2 \quad (5)$$

where for simplicity we have only considered up to 2nd order dispersion and neglected self-steepening and the SEWA correction to the dispersion. We will come back to this point later. Fourier transforming Eq. (5) and using the Fourier transform pair $\tilde{\phi}_2(\Omega) = \mathcal{F}[\phi_2](\Omega) \equiv (2\pi)^{-1/2} \int_{-\infty}^{\infty} d\tau e^{i\Omega\tau} \phi_2(\tau)$ and $\phi_2(\tau) = \mathcal{F}^{-1}[\tilde{\phi}_2](\tau) \equiv (2\pi)^{-1/2} \int_{-\infty}^{\infty} d\Omega e^{-i\Omega\tau} \tilde{\phi}_2(\Omega)$ the ODE (5) becomes simply $(\Omega^2 \delta_2^{(2)} - \Omega d'_{12} + \Delta k') \tilde{\phi}_2(\Omega) = -\Delta k'^{1/2} N_{\text{SHG}} \mathcal{F}[U_1^2](\Omega)$, so we can solve it in the frequency domain as

$$\tilde{\phi}_2(\Omega) = -(2\pi/\Delta k')^{1/2} N_{\text{SHG}} \tilde{R}(\Omega) \mathcal{F}[U_1^2](\Omega), \quad \tilde{R}(\Omega) \equiv \frac{\Delta k' (2\pi)^{-1/2}}{\delta_2^{(2)} \Omega^2 - d'_{12} \Omega + \Delta k'} \quad (6)$$

We now use the convolution theorem, so that in the time domain Eq. (6) becomes

$$\phi_2(\tau) = -\frac{N_{\text{SHG}}}{\sqrt{\Delta k'}} \int_{-\infty}^{\infty} ds R(s) U_1^2(\xi, \tau - s) \quad (7)$$

where the nonlocal response function in the time domain is $R(\tau) = \mathcal{F}^{-1}[\tilde{R}(\Omega)]$. This result shows that in the cascading limit the SH is affected by the FW in a nonlocal manner.

The next step is to calculate $R(\tau)$. To do this it is convenient to rewrite \tilde{R} in Eq. (6) as

$$\tilde{R}(\Omega) = (2\pi)^{-1/2} \frac{\Omega_a'^2 + s_b \Omega_b'^2}{(\Omega - \Omega_a')^2 + s_b \Omega_b'^2} \quad (8)$$

where we have introduced the dimensionless frequencies and the sign parameters

$$\Omega_a' = d'_{12}/2\delta_2^{(2)}, \quad \Omega_b' = |\Delta k'/\delta_2^{(2)} - \Omega_a'^2|^{1/2} \quad (9a)$$

$$s_a = \text{sgn}[\Omega_a'], \quad s_b = \text{sgn}[\Delta k'/\delta_2^{(2)} - \Omega_a'^2] \quad (9b)$$

The advantage of this notation is that it is now easy to characterize the roots of the polynomial in the denominator, which is important when we later will generalize to HOD.

When $s_b = +1$ Eq. (8) becomes a Lorentzian centered in Ω_a' and with the FWHM $2\Omega_b'$, see Fig. 2(b). The roots in the denominator of Eq. (8) are complex $\Omega = \Omega_a' \pm i\Omega_b'$. The temporal response function, $R_+(\tau)$, can readily be calculated by taking the inverse Fourier transform¹

$$R_+(\tau) = \frac{\tau_a^2 + \tau_b^2}{2\tau_a^2 \tau_b} \exp(-is_a \tau/\tau_a) \exp(-|\tau|/\tau_b) \quad (10)$$

where we have introduced the dimensionless characteristic nonlocal time scales

$$\tau_a = |\Omega_a'|^{-1} = |2\delta_2^{(2)}/d'_{12}|, \quad \tau_b = \Omega_b'^{-1} = |\Delta k'/\delta_2^{(2)} - \Omega_a'^2|^{-1/2} \quad (11)$$

The localized nature of Eq. (10) is shown in Fig. 2(a), and τ_b controls the width of $|R_+|$ while τ_a is the period of the phase oscillations. We note that Eq. (6) is defined so $\int_{-\infty}^{\infty} d\tau R_+(\tau) = 1$.

¹Note: on dimensional form $\mathcal{R}(t) = R(t/T_{\text{in}})/T_{\text{in}}$, which is independent on T_{in} since one must replace $\tau_{a,b}$ with the dimensional equivalent $t_{a,b} = \tau_{a,b} T_{\text{in}}$ in Eqs. (10,12). Instead in the frequency domain both \tilde{R} and \mathcal{R} are dimensionless.

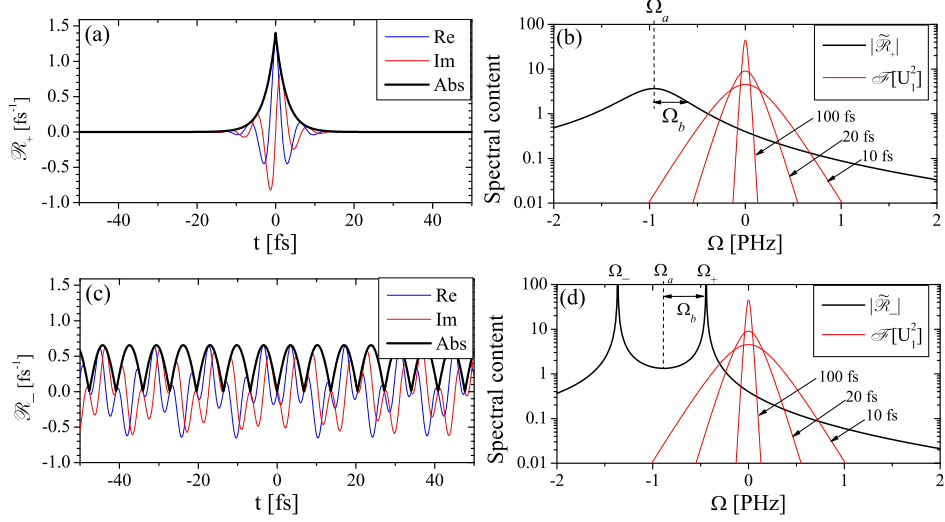


Fig. 2. The nonlocal response functions in the (a,b) stationary regime ($s_b = 1$) and (c,d) nonstationary regime ($s_b = -1$) as calculated for the simulation parameters in Fig. 1. The cusp in the origin of $|\mathcal{R}_\pm(t)|$ is typical for a Lorentzian response function. The spectral content of $U_1^2 = \text{sech}^2(t/T_{\text{in}})$ having 100, 20, and 10 fs FWHM duration is shown in (b,d).

When $s_b = -1$, $\tilde{R}(\Omega)$ has two simple poles at $\Omega = \Omega'_a \pm \Omega'_b \equiv \Omega'_\pm$, making $\tilde{R}(\Omega)$ diverge as shown in Fig. 2(d). Then $R_-(\tau) = \mathcal{F}^{-1}[\tilde{R}_-(\Omega)]$ exists as a Cauchy principal value giving

$$R_-(\tau) = \frac{\tau_a^2 - \tau_b^2}{2\tau_a^2\tau_b} \exp(-is_a\tau/\tau_a) \sin(|\tau|/\tau_b) \quad (12)$$

In contrast to R_+ , this response function is not localized but instead is oscillatory as a consequence of the two poles in $\tilde{R}_-(\Omega)$ [see the example shown in Fig. 2(c)].

Now, using Eq. (6) with the ansatz (4) and plugging it into Eq. (1a) we arrive at Eq. (3) under the aforementioned approximations. This essentially shows the central result of Ref. [10], namely that due to the cascaded quadratic nonlinearity the FW can be described by a generalized NLSE with a nonlocal temporal response in the Kerr-like SPM term. In Ref. [18] the nonstationary regime was defined as when GVM effects prevent the build-up of a nonlinear phase shift, which when applied to soliton compression consequently results in poor compression [6]. Based on the nature of the nonlocal response functions, we can now clarify that the boundary to the stationary regime is when s_b changes sign, which in dimensional units $\Delta k = \Delta k_{\text{sr}}$, where

$$\Delta k_{\text{sr}} = \frac{d_{12}^2}{2k_2^{(2)}} \quad (13)$$

Thus, to be in the stationary regime the phase-mismatch must be significantly large, $\Delta k > \Delta k_{\text{sr}}$. When GVM is weak compared to the phase mismatch then $s_b = +1$, and the response function (R_+) is monotonously decaying in magnitude: the convolution in the Kerr-like SPM term in Eq. (3) provides a finite temporal response. Therefore this must correspond to the stationary regime. Instead when GVM is strong compared to the phase mismatch then $s_b = -1$, and the response function (R_-) is oscillating and non-decaying: the temporal response from the convolution is no longer finite. Thus, this must correspond to the nonstationary regime.

Finally, to include the influence of self-steepening in the nonlocal theory, Eq. (17) would have the operator \hat{S}'_1 acting on all nonlinear terms and Eq. (5) would have the operator \hat{S}'_2 acting on the RHS. In frequency domain we may thus use a steepening-corrected response function $\tilde{R}^{\text{ss}}(\Omega) \equiv \tilde{R}'(\Omega)[1 + (\omega_2 T_{\text{in}})^{-1}\Omega]$. This does not change the transition value Δk_{sr} . Lastly, the NLS-like nonlocal equation (17) will have the operator \hat{S}'_1 acting on all nonlinear terms. It should also be stressed that self-steepening can affect the Raman-like term in Eq. (17) [20], but this effect does not appear in the nonlocal model used here because this would require taking into account higher-order perturbation terms [*i.e.*, making a more elaborate ansatz than Eq. (4)].

4. The weakly nonlocal limit

The nonlocal response in Eq. (3) can be better understood in the weakly nonlocal limit, where the width of the nonlocal response function is much narrower than the width of U_1^2 . The resulting simplified equation gives a better physical insight [22], and is important because it governs the initial dynamics (until pulse compression makes U_1 so short that the nonlocal response is no longer weak). We evaluate the convolution in the frequency domain $\int_{-\infty}^{\infty} ds R(s) U_1^2(\xi, \tau - s) = \int_{-\infty}^{\infty} d\Omega e^{-i\Omega\tau} \tilde{R}(\Omega) \mathcal{F}[U_1^2](\Omega)$ for convenience. In the weakly nonlocal limit $\tilde{R}(\Omega)$ is approximated by a 1st order expansion around $\Omega = 0$, where $\mathcal{F}[U_1^2](\Omega)$ is non-vanishing. This holds when $\tilde{R}(\Omega)$ varies slowly compared to $\mathcal{F}[U_1^2](\Omega)$. In this case

$$\tilde{R}(\Omega) \mathcal{F}[U_1^2](\Omega) \simeq \left[\tilde{R}(\Omega = 0) + \Omega \frac{d\tilde{R}}{d\Omega} \Big|_{\Omega=0} \right] \mathcal{F}[U_1^2](\Omega) \quad (14)$$

which in the time domain equivalently is $R(s) U_1^2(\xi, \tau - s) \simeq R(s) [U_1^2(\xi, \tau) - s \partial U_1^2(\xi, \tau) / \partial \tau]$. However, in the nonstationary regime the integration is done over two simple poles located on the Ω -axis. Using the residue theorem the frequency integral $\int_{-\infty}^{\infty} d\Omega e^{-i\Omega\tau} \tilde{R}(\Omega) \mathcal{F}[U_1^2](\Omega)$ can be evaluated as a contour integral, giving a contribution from the Cauchy principal value of the integral, and a contribution from deforming the integration contour around the poles on the real Ω -axis. The residual contributions from the poles to the frequency integral are [23]

$$\rho(\tau, U_1) = i \text{sgn}(\tau) \sqrt{\frac{\pi}{2}} \frac{\tau_a^2 - \tau_b^2}{2\tau_a^2\tau_b} \left[e^{-i\tau\Omega'_+} \mathcal{F}[U_1^2](\Omega'_+) - e^{-i\tau\Omega'_-} \mathcal{F}[U_1^2](\Omega'_-) \right] \quad (15)$$

which consist of an oscillatory component in form of complex exponentials with frequencies Ω'_\pm each weighted by the spectral strength of U_1^2 at that frequency. Thus, the influence of this contribution becomes important when the FW is short enough for its spectrum to cover the range, where Ω'_\pm are located, see Fig. 2(d). Using Eq. (15) and $(2\pi)^{1/2} \tilde{R}(0) = 1$ and $(2\pi)^{1/2} d\tilde{R}/d\Omega|_{\Omega=0} = 2\Omega'_a / (\Omega_a^2 + s_b \Omega_b^2)$, the nonlocal convolution is

$$\int_{-\infty}^{\infty} ds R(s) U_1^2(\xi, \tau - s) \simeq U_1^2 + i s_a \tau_{R,\text{SHG}} U_1 \frac{\partial U_1}{\partial \tau} + \frac{1 - s_b}{2} \rho(\tau, U_1) \quad (16)$$

Now introducing the effective soliton number $N_{\text{eff}}^2 = N_{\text{SHG}}^2 - N_{\text{Kerr}}^2$, Eq. (3) becomes

$$\left[i \frac{\partial}{\partial \xi} - \frac{1}{2} \frac{\partial^2}{\partial \tau^2} \right] U_1 - N_{\text{eff}}^2 U_1 |U_1|^2 = N_{\text{SHG}}^2 \left[i s_a \tau_{R,\text{SHG}} |U_1|^2 \frac{\partial U_1}{\partial \tau} + \frac{1 - s_b}{2} U_1^* \rho(\tau, U_1) \right] \quad (17)$$

The first term on the RHS is a GVM-induced Raman-like perturbation caused by the cascaded SHG nonlinearity. It is Raman-like due to the asymmetry of R_\pm [10], stemming from the phase term $\exp(-i s_a \tau / \tau_a)$ in Eqs. (10) and (12). It has the characteristic dimensionless time $\tau_{R,\text{SHG}} \equiv 4|\Omega'_a| / (\Omega_a^2 + s_b \Omega_b^2) = 2|d'_{12}| / \Delta k'$ [6, 10, 11, 18], which on dimensional form reads

$$T_{R,\text{SHG}} = \tau_{R,\text{SHG}} T_{\text{in}} = 2|d_{12}| / \Delta k \quad (18)$$

The direct dependence on the GVM-parameter d_{12} implies that the Raman-like perturbation disappears in absence of GVM. Equation (17) was also derived for the stationary regime $s_b = 1$ in Ref. [10]², obviously without the contribution $U_1^* \rho(\tau, U_1)$.

Eq. (17) is a very strong result: It states that in the weakly nonlocal limit the effective soliton number N_{eff} can be used in the scaling laws of [11] to predict, e.g., the optimal compression point. Previously these scaling laws were thought to hold only in the stationary regime [10, 11]. The result also tells us that in the weakly nonlocal limit, a central observation of Ref. [6] is confirmed: for a given, fixed value of Δk , the Raman-like effect of the first term of the RHS of Eq. (17) becomes increasingly significant with increasing N_{SHG}^2 , thus limiting the possible compression ratio. However, it is now clear that in the nonstationary regime, the Raman-like distortion is accompanied by an oscillatory perturbation term $U_1^* \rho(t, U_1)$ which also increases with N_{SHG}^2 . In both the stationary and nonstationary regimes the Raman-like distortions place a limitation on the maximum soliton order, but in the nonstationary regime both terms on the RHS of Eq. (17) distort the compression, and the combined effect is more severe, a result that is also confirmed by numerical simulations below. On the other hand, it is also obvious that for low soliton numbers these detrimental effects are weak and it is actually possible to observe clean compressed pulses even in the nonstationary regime, as observed by both numerical simulations as well as experiments [3, 5].³ This is also apparent in Eq. (15) where the oscillations can be neglected if $\mathcal{F}[U_1^2](\Omega'_\pm)$ is vanishing, *i.e.*, if the compressed pulse duration is long enough.

In the stationary regime the characteristic time scale that decides the strength of the nonlocal response is $t_b = \tau_b T_{\text{in}}$. The weakly nonlocal approximation applies when $t_b \ll \Delta t$, where Δt is the FW pulse duration. But when does it apply in the nonstationary regime? We know that the width $\Delta\Omega$ of $\mathcal{F}[U_1^2]$ is $\Delta\Omega \propto \Delta t^{-1}$. Referring to Fig. 2(d) we must require that the positions of the two poles Ω_\pm be sufficiently far away from the frequency range, where $\mathcal{F}[U_1^2]$ is non-vanishing, *i.e.*, $|\Omega_\pm| \gg \Delta\Omega$. In physical units this implies that the weakly nonlocal limit in the nonstationary regime can be expressed by the requirement $\Delta t \gg t_a t_b / |t_a - t_b|$.

Let us evaluate this requirement. It is important to notice from Eq. (11) that t_b diverges at the transition Δk_{sr} , see also Fig. 3(a). Thus, in the nonstationary regime the requirement $\Delta t \gg t_a t_b / |t_a - t_b|$ holds even for quite short pulses as long as t_a and t_b are not too similar. This is generally true close to the transition Δk_{sr} , while away from the transition $t_b \simeq t_a$ because Δk gets small, see Eq. (11) and Fig. 3(a). In this case we can no longer be sure to be in the weakly nonlocal limit. In the stationary regime the system will initially be in the weakly nonlocal limit $\Delta t \gg t_b$ except close to the transition Δk_{sr} , where t_b diverges. It is interesting to notice that the weakly nonlocal limit in the stationary regime is well away from the transition Δk_{sr} , while in the nonstationary regime it is close to the transition Δk_{sr} . We finally remark that t_a also may diverge when GVM is negligible. This implies that the factor $e^{-is_a \tau / \tau_a} = 1$, so $R(\tau)$ becomes real and symmetric. Thus, the 1st order correction on the RHS of Eq. (17) disappears because the Raman-like perturbation vanishes ($T_{R,\text{SHG}} = 0$) and a 2nd order correction must be made.

5. Numerical results and discussion

We will now apply the results of the nonlocal theory to understand realistic numerical simulations of Eq. (1). It is important to stress that the theory neglects Kerr XPM effects and that the coherence length is the shortest length scale in the system. This latter requirement implies that the system can *initially* be well described by the nonlocal theory, but as the pulse is compressed the GVM (and other length scales) can become so short that this is no longer true. Therefore the accuracy of the nonlocal model will not always be enough to accurately predict the outcome of the numerical simulations and the experiments. However, since the nonlocal model often will

²The factor s_a on the RHS of Eq. (17) was unfortunately lost during the proofs in Eq. (12) of Ref. [10].

³These experiments were actually done in the nonstationary regime according to the nonlocal theory.

be an adequate approximation for a large part of the propagation through the nonlinear medium, we can still use it to understand the temporal dynamics until that potentially happens.

We will now show that there are two main categories of compression limitations.

1. Effects limiting phase-mismatch range where compression is possible and efficient
 - (a) In the nonstationary regime $\Delta k < \Delta k_{\text{sr}}$ the oscillatory nonlocal response function implies that compression is inefficient unless the soliton order is very low.
 - (b) Competing cubic nonlinearities pose an upper limit Δk_c [10, 11] beyond which $N_{\text{eff}} < 1$ always. Close to this limit detrimental cubic XPM effects are observed.
2. Effects limiting the compression for a selected phase-mismatch value
 - (a) The effective soliton order $N_{\text{eff}} = (N_{\text{SHG}}^2 - N_{\text{Kerr}}^2)^{1/2}$ controls in the weakly nonlocal limit the compression factor $f_C = T_{\text{in}}/\Delta t_{\text{opt}} = 4.7(N_{\text{eff}} - 0.86)$ [11].
 - (b) Nonlocal effects. In the stationary regime Δt_{opt} is limited by the strength of the nonlocal response function t_b . In the nonstationary regime Δt_{opt} is limited by the characteristic time $T_{R,\text{SHG}}$ of the GVM-induced Raman-like perturbation.
 - (c) Propagation effects pertaining solely to the FW, such as higher-order dispersion, the Raman effect (negligible in nonlinear crystals) and cubic self-steepening.
 - (d) Competing cubic nonlinearities necessitate large quadratic soliton orders N_{SHG} , which increases detrimental nonlocal effects such as the Raman-like perturbation.

The numerical simulations of Eqs. (1) were performed using a β -barium-borate crystal (BBO) as the quadratic nonlinear medium. The phase mismatch was changed through angle-tuning of the crystal in a type I SHG configuration (implying $B = 2/3$, see [11] for further details), and we are interested in $\Delta k > 0$, for which GVD is normal and $d_{12} < 0$ (so $s_a < 0$).

Figure 3 summarizes simulations of pulse compression of a 200 fs FWHM pulse centered at $\lambda_1 = 1064$ nm: the FW pulse duration at the point of optimal compression Δt_{opt} (dark circles) is plotted as the phase mismatch Δk is swept. The strength of the cascaded quadratic nonlinearity $N_{\text{SHG}}^2 \propto \Delta k^{-1}$, while the Kerr nonlinearity remains unchanged. However, in the plot we keep $N_{\text{eff}} = 8$ fixed by adjusting the input intensity $I_{\text{in}} = \frac{1}{2}n_1 \epsilon_0 c \mathcal{E}_{\text{in}}^2$.⁴ This implies that the scaling law [11] predicts equal compression everywhere (dotted orange line). While we do observe such a compression in the regime around $\Delta k = 50 \text{ mm}^{-1}$ [this example is shown in Fig. 1(a)-(b), and also in Fig. 4], away from this point the compression becomes sub-optimal.

Before explaining the results in detail, we must mention that the nonlocal time scales plotted in Fig. 3(a) are not those of Eq. (11); these only take into account up to second-order dispersion (dispersion order $m_d = 2$), while in the numerical simulations the dispersion is calculated exactly from the Sellmeier equations [11], and subsequently corrected in the SEWA framework up to 30th order [11]. This poses a correction on the nonlocal time scales as well as the transition to the nonstationary regime, which was calculated numerically: we replaced the polynomial in the denominator of \tilde{R} in Eq. (6) with $\hat{D}_{2,\text{eff}}$ (evaluated in frequency domain). The transition to the nonstationary regime happens when a root-pair switches from being each others complex conjugate to being purely real and nondegenerate. Then $\Omega_{a,b}$ and $t_{a,b}$ can be extracted from these roots. The transition to the stationary regime (13) is now simply found when t_b diverges. Fig. 3 shows for comparison also t_b calculated with $m_d = 2$, *i.e.*, using Eq. (11).

The degrading compressor performance observed for large Δk in Fig. 3(a) is caused by the onset of XPM-effects. As Δk is increased the cascaded quadratic nonlinearity is reduced, so in

⁴This is a typical experimental situation, because the optimal compression point z_{opt} scales with N_{eff} [11], and since the nonlinear crystal length is a constant parameter one adjusts the intensity so z_{opt} coincides with the crystal length.

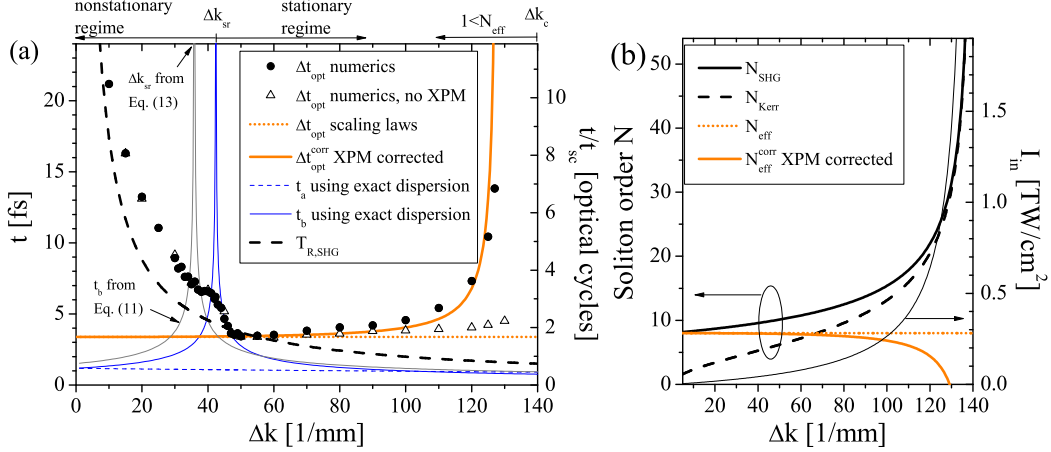


Fig. 3. Data from numerical simulations as in Fig. 1 for different values of Δk . (a) The FW duration $\Delta t_{\text{opt}} = \Delta t_{\text{opt}}^{\text{FWHM}}/1.76$ at $z = z_{\text{opt}}$ is shown both for the full SEWA model (1), and when neglecting the Kerr XPM terms. The lines show the nonlocal time scales $t_{a,b} = T_{\text{in}} \tau_{a,b}$, the characteristic Raman-like time $T_{R,\text{SHG}} = 2|d_{12}|/\Delta k$, and the predicted Δt_{opt} from the scaling laws [11] as well as the predicted $\Delta t_{\text{opt}}^{\text{corr}}$ when correcting for XPM effects on N_{eff} . t_b as calculated using only up to second-order dispersion ($m_d = 2$, gray curve) is also shown. The right ordinate shows time normalized to the single-cycle pulse duration $t_{\text{sc}} = 2.0$ fs. (b) The SHG and Kerr soliton numbers required to have $N_{\text{eff}} = 8$ fixed, achieved by adjusting I_{in} . The corrected effective soliton number due to XPM effects $N_{\text{eff}}^{\text{corr}}$ is also shown.

order to keep $N_{\text{eff}} = 8$ the input intensity I_{in} must be increased, see Fig. 3(b). Eventually the required intensity diverges because Δk approaches the so-called upper limit of the compression window Δk_c , beyond which $N_{\text{eff}} < 1$ always [10, 11]. As I_{in} becomes large so does the input beam fluence $\Phi_{\text{in}} = 2T_{\text{in}}I_{\text{in}}$, and this makes XPM effects more pronounced; as shown in [11] above a critical fluence of $\Phi_c = 33 \text{ mJ/cm}^2$ the onset of compression in a BBO is not $N_{\text{eff},c} = 1$ – as one would expect from the NLS-like equation (3) – but can approximately be described by the scaling law $N_{\text{eff},c} = 1 + \Delta N_{\text{eff}}$, with $\Delta N_{\text{eff}} = \Phi_{\text{in}}/[\Phi_c(1 + \Phi_c/\Phi_{\text{in}})]$ as the delay in onset. The delay is caused by the XPM term creating an intensity dependent self-focusing phase-shift in addition to the one already created by the Kerr SPM term. The immediate consequence is that we can no longer expect the compression factor of $f_c = 33.5$ predicted from $N_{\text{eff}} = 8$; instead we must use a corrected effective soliton number $N_{\text{eff}}^{\text{corr}} = N_{\text{eff}} - \Delta N_{\text{eff}}$ [see Fig. 3(b)], which for high fluences then will give a reduced compression performance. Figure 3(a) shows Δt_{opt} as predicted from the scaling laws for $N_{\text{eff}} = 8$ (dotted orange line), together with the corrected $\Delta t_{\text{opt}}^{\text{corr}}$ as calculated using $N_{\text{eff}}^{\text{corr}}$ (solid orange line). As expected for high Δk values $\Delta t_{\text{opt}}^{\text{corr}}$ starts to deviate from Δt_{opt} . Importantly, it seems to describe very accurately the compression performance observed numerically. An example of how the pulse looks like in this regime is shown in Fig. 4 ($\Delta k = 125 \text{ mm}^{-1}$, blue curve). The compressed pulse is longer (18 fs FWHM) and we also checked that it compresses later than what one would expect with $N_{\text{eff}} = 8$. These values correspond very well to what the reduced soliton number $N_{\text{eff}}^{\text{corr}} \simeq 3$ predicts through the scaling laws. Thus, XPM strongly degrades compression when the beam fluence becomes large. This is also confirmed by the simulations shown with open circles in Fig. 3(a), for which XPM effects were turned off: only a weak degradation in compression is seen for high Δk .

For $\Delta k = 43 - 50 \text{ mm}^{-1}$ the limit to compression is determined by the strength of the nonlocal

response function. Close to the transition to the nonstationary regime t_b becomes large, so the nonlocal response \mathcal{R}_+ is very broad. Initially, however, the 200 fs FWHM input pulse sees only a weakly nonlocal response. As the pulse compresses the nonlocal response becomes strongly nonlocal, whereby the NLS-like model (3) reduces to a linear Schrödinger equation having a potential defined by the response function [19,22,24–26]. The pulse cannot be narrower than the width of this potential given by t_b , which explains the behaviour observed for phase-mismatch values just above Δk_{sr} . This has also been observed for spatial nonlocal solitons [19,22,24–26].

For $\Delta k < 42 \text{ mm}^{-1}$ the system is in the nonstationary regime and as Δk is reduced Δt_{opt} increases as Δk^{-1} . The compression limit does therefore not follow t_b , but instead follows the characteristic Raman-like time $T_{R,\text{SHG}} = 2|d_{12}|/\Delta k$ quite closely. Indeed some physical explanation can be extracted from this parameter, since it namely represents the pulse duration, where the GVM length $L_{\text{GVM}} = \Delta t/|d_{12}|$ becomes shorter than the coherence length $L_{\text{coh}} = \pi/\Delta k$. Intuitively it seems logical that the compressed pulse duration hit a limit when the GVM length is equal to the coherence length: the cascaded nonlinear interaction can no longer build up the phase shift because the GVM will remove the FW and SH from each other before even one cascaded cycle is complete. It is interesting to note that arguments similar to these were initially used to define the nonstationary regime [14, 18], and it was already there clear that compression was limited in the same way as shown here. These studies were, as mentioned before, carried out in the nonstationary regime as defined by the nonlocal analysis, so the results corroborate each other. Another important result from the nonlocal analysis is that there is an oscillatory contribution in the nonstationary regime $\rho(\tau, U_1)$, see Eq. (15). When we consider a pulse that gets shorter and shorter, the strength of $\mathcal{F}[U_1^2](\Omega_{\pm})$ becomes larger and larger [see Fig. 2(d)], and so we start in the present case to observe oscillations with frequency $\Omega_+ = \Omega'_+/T_{\text{in}}$ (since Ω_+ in the present example is the frequency closest to origin). That means that the soliton sees an oscillating potential with period $\propto |\Omega_+|^{-1}$, so we would expect that the pulse duration can never go below $|\Omega_+|^{-1}$. This explains very well why the pulse duration increases in the nonstationary regime when Δk is decreased. It should also be mentioned that in the nonstationary regime $T_{R,\text{SHG}} = |\Omega_+^{-1} + \Omega_-^{-1}|$, which therefore supports this explanation. Note that no data points below $\Delta k = 10 \text{ mm}^{-1}$ are shown because the cascading limit breaks down there [12].

To better understand the difference between the stationary and nonstationary regimes, Fig. 4(a) shows examples of compressed pulses. For $\Delta k = 50 \text{ mm}^{-1}$ a 6.3 fs FWHM compressed pulse is observed as expected from the scaling laws, while as the transition to the nonstationary regime is approached ($\Delta k = 43 \text{ mm}^{-1}$) the pulse compression is limited by the nonlocal potential of strength t_b . Once inside the nonstationary regime, the pulse not only becomes compressed poorly, but trailing oscillations are evident. The corresponding FW and SH wavelength-spectra are shown in Fig. 4(b) and (c). For $\Delta k = 50 \text{ mm}^{-1}$ both the FW and SH spectra are very flat, except for a spectral FW peak and corresponding spectral SH hole. As we explain below these peaks are actually dispersive waves. Closer to the transition ($\Delta k = 43 \text{ mm}^{-1}$) the SH spectrum develops a peak because $\tilde{\mathcal{R}}_+(\Omega)$ here is a very narrow Lorentzian. Inside the nonstationary regime a distinct red-shifted peak grows up in the SH spectrum, which can be explained by the nonlocal theory since the spectral peak sits at the frequency Ω_+ . In turn, close to the transition ($\Delta k = 41 \text{ mm}^{-1}$) the FW has a corresponding spectral hole at $\omega_1 + \Omega_+$, while further from the transition ($\Delta k = 30 \text{ mm}^{-1}$) it becomes a spectral peak. To confirm this, we show in Fig. 4(d) the red-shifted holes/peaks found numerically versus Δk , with an impressive agreement with the nonlocal theory. This FW spectral hole/peak is the main limitation to the pulse compression in the nonstationary regime.

The FW spectra in Fig. 4(b) have pronounced peaks around $\lambda = 2.9 \text{ }\mu\text{m}$. To understand this we observed that the FW dispersion operator in the frequency domain $\hat{D}_1(\Omega) = \sum_{m=2}^{\infty} m!^{-1} \Omega^m k_1^{(m)}$ changes sign and for $\lambda_1 = 1.064 \text{ }\mu\text{m}$ becomes negative beyond the dotted

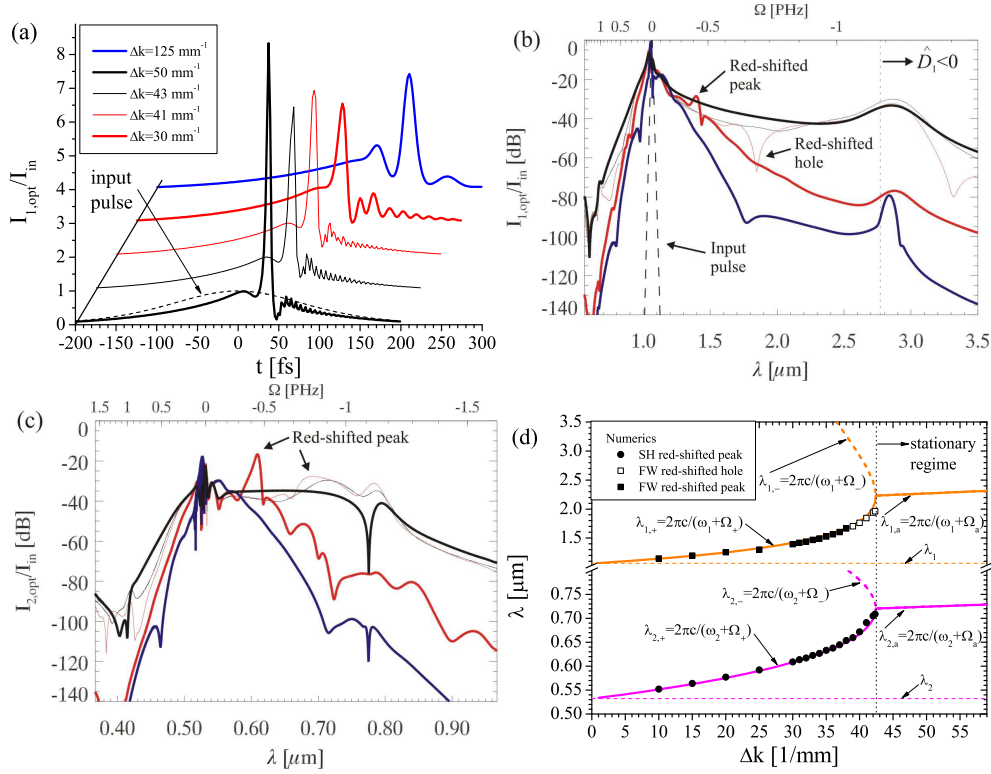


Fig. 4. Data from the numerical results in Fig. 3 for selected values of Δk : (a) $|U_1|^2$ at $z = z_{\text{opt}}$ versus time, (b) the corresponding FW and (c) SH wavelength spectra. Only up to $\lambda = 3.5 \mu\text{m}$ is shown in (b) since this is the edge of the transparency window of BBO [21]. The plots for $\Delta k = 50 \text{ mm}^{-1}$ and 30 mm^{-1} are the cuts in Fig. 1 at $z = z_{\text{opt}}$. (d) The position of the red-shifted spectral peaks in the nonstationary regime. The symbols are the results of numerical calculations while the lines are the predictions of the nonlocal theory.

line in Fig. 4. Based on previous results from the NLSE [27–29] at this point the compressed soliton should therefore be phase matched to a linear dispersive wave. Such dispersive waves have not been observed before with cascaded quadratic nonlinearities, but their appearance further underlines the analogy between soliton compression with cascaded quadratic nonlinearities and with cubic nonlinear media. The wavelength of the dispersive wave λ_{dw} seems not to change as Δk is varied, which is due to the FW dispersion being independent on the crystal angle. Instead λ_{dw} changes strongly with the soliton frequency, but the soliton-frequency blue shifts observed in the simulations were quite small and similar (around 30-40 THz). The solitons are blue shifted because $\Delta k > 0$ and $s_a < 0$ and the shifts explain why the dispersive waves are slightly red-shifted compared to the dotted line. The dispersive waves can also be noted in Fig. 1(b,d). They do not emerge before the pulse is compressed, because their strength is related to the spectral strength of the soliton to which they are coupled [29].

What happens when the effective soliton order in the stationary regime is pushed to create single-cycle pulses? In a previous study it was found that the GVM-induced Raman-like perturbation beyond some optimal soliton order starts to dominate and makes the compressed pulse asymmetric, while the peak intensity drops (Fig. 1 in Ref. [6], where $\Delta k = 16 \pi/\text{mm}$). These

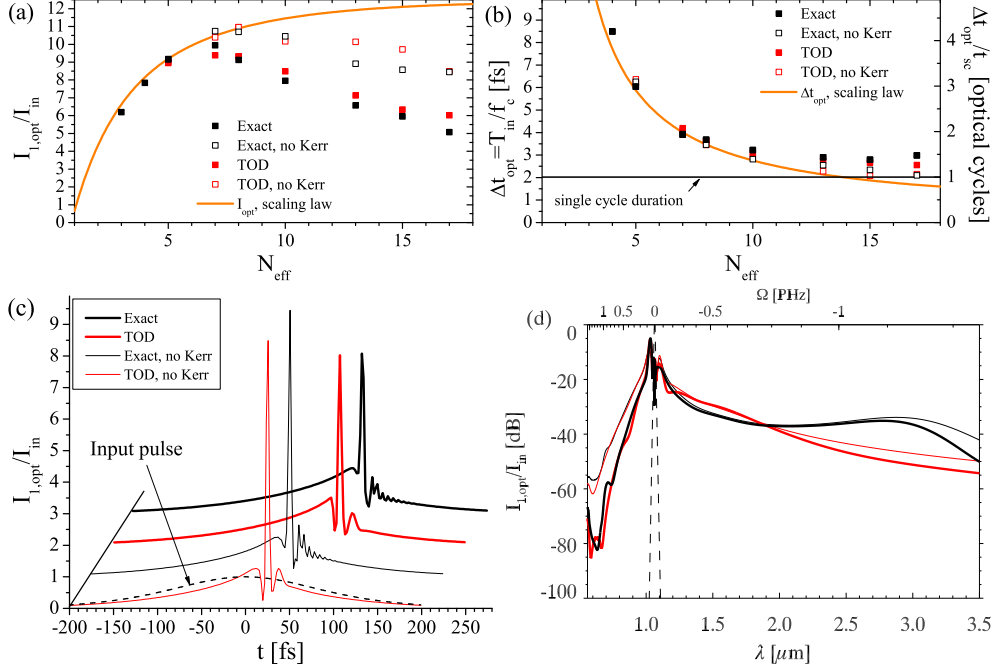


Fig. 5. Results of pulse compression simulations as in Fig. 3, taking $\Delta k = 60 \text{ mm}^{-1}$ and varying N_{eff} . (a) and (b) show $I_{1,opt}/I_{in}$ and Δt_{opt} when using exact dispersion ($m_d = \infty$) and when including up to TOD ($m_d = 3$), as well as the same simulations without competing Kerr nonlinearities. The orange curves are the predicted values from the scaling laws [11], corrected for XPM. (c) and (d) show FW time and spectral profiles for $N_{eff} = 17$.

results are confirmed in Fig. 5(a), showing the peak intensity of the compressed pulse versus N_{eff} for $\Delta k = 60 \text{ mm}^{-1}$. Beyond $N_{eff} = 8$ the pulse compression deviates from the prediction of the scaling law, even for the simulations including only up to third order dispersion (TOD, *i.e.*, dispersion order $m_d = 3$), or neglecting the competing Kerr nonlinearities. However, the compressed pulse duration Δt_{opt} , shown in Fig. 5(b), decreases even beyond this point of maximum intensity. The explanation is that $\Delta t_{opt} = T_{in}/f_c$ in (b) is determined by the compression factor f_c alone, while the intensity in (a) is $I_{1,opt}/I_{in} = f_c Q_c$, where Q_c is the compressed pulse quality relating the energy of the central spike to the initial pulse energy. Around $N_{eff} = 17$ the compressed pulse is quite close to the single-cycle regime. The time profiles for this case are shown in Fig. 5(c). The simulations without Kerr nonlinearities (so $N_{SHG} = N_{eff} = 17$) actually predict single-cycle compressed pulses, while turning on the Kerr nonlinearities the compressed pulses are no longer single-cycle but increase to 1.5 optical cycles. Notice also that the pulses with Kerr nonlinearities are more asymmetric. This asymmetry is caused by the GVM-induced Raman-like perturbations [1st term on the RHS of Eq. (17)] as pointed out in Ref. [6]. Since this effect stems from the quadratic nonlinearities it must be stressed that they are also affecting the single-cycle pulses obtained without Kerr nonlinearities. However, the difference is that there $N_{SHG} = 17$ while with Kerr nonlinearities $N_{SHG} = 22.9$ must be chosen to have $N_{eff} = 17$. Therefore the strength of the Raman-like perturbation, which scales as N_{SHG}^2 , is much stronger when including the competing Kerr nonlinearities leading to a more asymmetric pulse. We also note that the simulations with exact dispersion (no polynomial expansion, $m_d = \infty$) have fast

trailing oscillations, which are absent for the TOD simulations. The FW spectra in Fig. 5(d) offer an explanation: only with exact dispersion is there a spectral peak around $3 \mu\text{m}$; these are phase-matched dispersive waves. With TOD the spectrum is instead smooth because the phase-matching condition for the dispersive wave is pushed far into the infra-red.

Considering these results, a brief discussion on the effect on TOD in soliton compressors is fruitful. In fiber soliton compressors the most detrimental effect on pulse compression is the Raman self-scattering term, that comes from a non-instantaneous Kerr nonlinear response. As mentioned before, this effect can be neglected in nonlinear crystals. However, Chan and Liu showed that TOD can severely distort the pulse when GVD is small [30], while for larger GVD the TOD is less important for the pulse shape [31], and simply leads to a slowing down of the soliton. In this context the TOD effect observed here, namely that the phase-matching wavelength of the dispersive wave is shifted, is completely different. We also remark that in our simulations TOD is positive, and GVD is not small ($k_1^{(2)} \simeq 40 \text{ fs}^2/\text{mm}$ and $k_2^{(2)} \simeq 100 \text{ fs}^2/\text{mm}$).

Summing up, the GVM-induced Raman-like distortions prevents efficient compression at high soliton numbers (as previously found in Ref. [6]), and the competing cubic nonlinearities aggravates this effect. In addition, the presence of a dispersive wave prevented soliton compression to the single-cycle level. The dispersive wave disappears when only including up to TOD because the dispersion is no longer accurate in the region where the dispersive wave is observed, and this underlines the importance of including HOD in the numerics. An interesting case to study would be when a large dispersion control is possible, such as with photonic crystal fibers [32]. One could namely imagine that the dispersion could be engineered, so the phase-matching condition for the dispersive wave is pushed into the far IR-regime, allowing for further compression towards the single-cycle regime.

6. Conclusions

To summarize we have shown that the limits to compression in cascaded quadratic soliton compressors can in most cases accurately be understood from a nonlocal model, which describes the cascaded quadratic nonlinearity as a nonlocal Kerr-like self-phase modulation response.

In the stationary regime, where the nonlocal response is localized, one cannot compress pulses beyond the width (strength) of the nonlocal response function. When increasing the effective soliton order to potentially compress beyond single-cycle duration, the numerical simulations indicated that competing Kerr nonlinear effects were preventing single-cycle compressed pulses: Since the quadratic soliton number must be chosen much larger than without Kerr nonlinearities, this increases detrimental effects such as the GVM-induced Raman-like perturbation found using the nonlocal theory. Additionally it was found that higher-order dispersion can also prevent the observation of single-cycle compressed pulses. In particular, dispersive waves phase-matched to the compressed higher-order soliton caused trailing oscillations on the compressed pulse, eventually impeding further compression even at higher intensities.

In the nonstationary regime the nonlocal response function is oscillatory, and the convolution between the pulse and the nonlocal response function in the weakly nonlocal limit can elegantly be understood in the same way as in the stationary regime, except for an oscillatory contribution that causes trailing oscillations in the compressed pulse and severely degrades compression. The SH spectrum was found to be strongly red-shifted to a wavelength accurately predicted by the nonlocal theory. This spectral shift in turn induces a peak in the FW, which is the main compression limitation in the nonstationary regime. The compression limit was found to be the characteristic Raman-like response time of the cascaded process $T_{R,\text{SHG}}$, roughly the pulse duration for which the GVM and the coherence lengths become identical.

Another compression limit is set by the material Kerr nonlinearity, which makes compression possible only below a critical phase mismatch parameter, and requires large soliton orders for

successful compression. Thus, higher-order effects (XPM, higher-order dispersion and self-steepening) come into play and detrimental nonlocal effects are increased. The XPM effects were accurately accounted for by using a corrected (reduced) soliton number.

The present analysis will serve as a useful tool for further experimental progress in soliton compression using cascaded quadratic nonlinearities. We will now focus our attention to compression in a BBO at $\lambda_1 = 800$ nm, because GVM is much stronger than what was presented here. Thus we expect the nonlocal analysis to provide more insight into this case, in particular concerning the nonstationary regime, which is the dominating one at 800 nm.

M.B. acknowledges support from The Danish Natural Science Research Council (FNU, grant no. 21-04-0506).